

## Novel approach for early damage detection on rotor blades of wind energy converters

Stephan Zerbst<sup>a</sup>, Stavroula Tsiapoki\* and Raimund Rolfes<sup>b</sup>

*Institute of Structural Analysis, Leibniz Universität Hannover, Appelstr. 9A, Hannover, Germany*

*(Received February 9, 2012, Revised May 16, 2013, Accepted March 4, 2014)*

**Abstract.** Within this paper a new approach for early damage detection in rotor blades of wind energy converters is presented, which is shown to have a more sensitive reaction to damage than eigenfrequency-based methods. The new approach is based on the extension of Gasch's proportionality method, according to which maximum oscillation velocity and maximum stress are proportional by a factor, which describes the dynamic behavior of the structure. A change in the proportionality factor can be used as damage indicator. In addition, a novel deflection sensor was developed, which was specifically designed for use in wind turbine rotor blades. This deflection sensor was used during the experimental tests conducted for the measurement of the blade deflection. The method was applied on numerical models for different damage cases and damage extents. Additionally, the method and the sensing concept were applied on a real 50.8 m blade during a fatigue test in the edgewise direction. During the test, a damage of 1.5 m length was induced on the upper trailing edge bondline. Both the initial damage and the increase of its length were successfully detected by the decrease of the proportionality factor. This decrease coincided significantly with the decrease of the factor calculated from the numerical analyses.

**Keywords:** structural health monitoring; condition monitoring; wind turbine rotor blades

---

### 1. Introduction

The need for energy production through renewable sources, in combination with the environmental friendliness that wind turbines offer, has contributed to the increasingly high power generation from wind turbines. Therefore, the development in wind turbine design and fabrication has been strongly accelerated, resulting in an increase of the generated power and consequently the size of wind turbines. Turbine power has increased to 6 MW, while towers up to 126 meters average height and blades up to 65 meters length have become state of the art. A further step, that established a new dimension in energy production, is the construction of offshore wind farms.

The speed of a quickly growing market can often be responsible for lack of manufacturing quality and at the same time it can be the reason for too conservative structural design. The more factory output increases, the more difficult it is to maintain the level of manufacturing quality. At the same time, the development of rotor blades of wind turbines has rapidly grown to extremes.

---

\*Corresponding author, Ph.D. Student, E-mail: [s.tsiapoki@isd.uni-hannover.de](mailto:s.tsiapoki@isd.uni-hannover.de)

<sup>a</sup> Dr.-Ing., E-mail: [s.zerbst@isd.uni-hannover.de](mailto:s.zerbst@isd.uni-hannover.de)

<sup>b</sup> Professor, E-mail: [r.rolfes@isd.uni-hannover.de](mailto:r.rolfes@isd.uni-hannover.de)

Since the composite rotor blades are manufactured manually, quality within one blade type may vary widely and failure due to processing quality is likely. Most typical scenarios resulting from manufacturing and design reasons are damages like web debonding and bondline failure. Unlike an incidence of delamination of the composite material, these types of damage can seriously affect the structural integrity at a quite early stage of the rotor blades life cycle.

Some severe damages of rotor blades during operation have been documented (Ashley *et al.* 2007) (Caithness Windfarm Information Forum 2010) (Wind Watch 2010). For instance in May 2007, a 40 m blade collapsed and crashed around 60 kilometers north-east of the city of Leipzig, Germany, ending up only 60 m away from highway B183 (Claus 2007). Parts of the blade were catapulted up to 200 meter from the wind turbine. The *Micon* turbine was built only in 2003. When the blade collapsed, a team of service technicians was working on top of the turbine, while the wind speed was currently 30 m/s, which is equal to 11Bft. However, this fact is not sufficient to cause blade loss. It was assumed that the blade was damaged before this incident, whereas fatigue could not be eliminated as a possible reason.

The annual failure rate of wind turbines is documented to have a value of 0.2, which results to an average down time due to repair works of 5 days per failure, while it is deduced that the only structural components having major failure rates are blades (Hahn *et al.* 2006). All unforeseen malfunctions of the electrical or mechanical components that cause downtime of the wind turbine for repair or replacement works are designated as damage and are included in the annual failure rate. The process of repairing of wind turbine blades is always difficult, starting with visual inspections by technicians inside or even outside the blade and leading to the engineer's decision of the required work to be conducted afterwards. Furthermore, the lamination work, which is necessary for blade repair, requires time for preparation and time for processing, hardening and finishing the damage location before the turbine can be restarted again. Currently the loss of one hour of onshore turbine power, harvested on a 3.3 MW turbine at rated wind, is approximately 275€. As far as the offshore wind turbines are concerned, the costs are even higher, since the turbine has to be accessed by a ship. Finally, the use of fiber material and epoxy has to be done carefully, because it may affect the technician's health.

There are numerous arguments supporting the need for reliable damage detection systems, in order to reduce annual failure rates, the resulting down time and any necessary repair work on the turbine. Reliable condition-based maintenance concepts have to be developed to reduce the inspection frequency to the required minimum and to detect damages at an early stage. Costs can only be reduced as soon as reliable damage detection systems are available, which are robust in design and technically mature.

## 2. Basic design and fabrication of wind turbine blades

State of the art wind turbine blades are designed to have optimum aerodynamic properties. Thus, the blade shape starting from the root has to change from a cylindrical to an aerodynamic cross section, composed of leading and trailing edge. The cylindrical cross-section is needed in order to connect the blade to the hub, where pitch control is also located. At the root section a strong multi-axial, multilayered composite material is required, while screwed holes are used to realize the bolt connection to the hub (Gasch and Twele 2007). In Fig. 1 the basic design of a particular blade type is presented as an example.

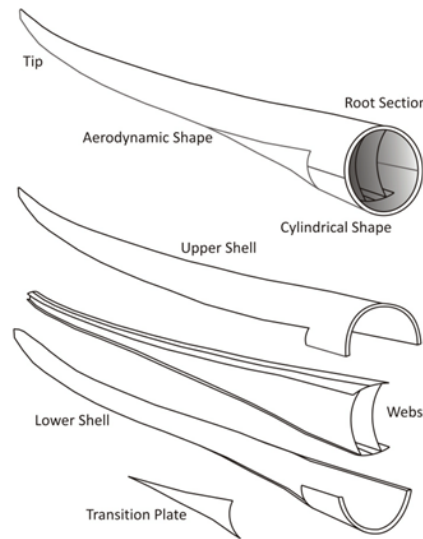


Fig. 1 Schematic diagram of an example blade design

For load-carrying reasons former smaller blade types were constructed with a box girder stretching from root to tip. Today most of the blades are designed having one, two or even more webs that extend across the whole length. These webs, together with the main girders, carry bending loads as well as torsional loads from the aerodynamic shells (upper and lower or suction and pressure side respectively), which are bonded on the upper and lower part of the webs and extend from the root section to the tip of the blade. Unlike the root section, sandwich elements are used along the aerodynamic shells (see Fig. 2). It is even possible to have webs that include sandwich layers (Thomson 2009). Depending on blade length and design, it might be necessary to have additional girders along highly loaded areas. In particular larger blades might need additional girders along the leading and trailing edge, beside the upper and lower main girders, in order to carry the loads to the root section, where the load is transferred to the hub.

Regardless of blade type or size, in the end these shells are glued together with resin along their bondlines. Within the first step of fabrication process the webs are bonded to the lower shell. Then the upper shell is positioned to be bonded as well. Hereby, a “blind bondline” arises between upper shell and upper girder of the webs, which can hardly be controlled in terms of bonding quality. This “blind bondline” is a potential position for damage initiation. Since blade lengths have increased to more than 60 m, the fabrication strategy is changing. Due to production time cost issues, smaller shell components are prefabricated and assembled during the final production step. Furthermore, transportation has become an important issue as well. Onshore construction sites can hardly be accessed when trucks have to deliver large blades of more than 60 m length, which have to be transported on federal and country roads. Therefore, German manufacturer Enercon has started to construct hybrid blades, made of both a composite and a steel section, which are assembled at the construction site.

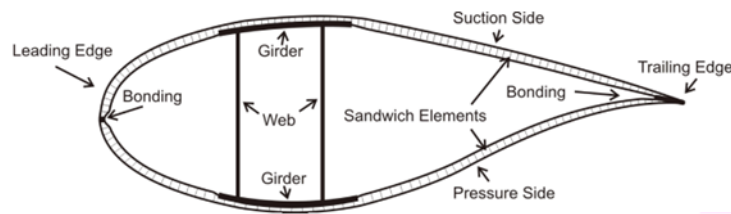


Fig. 2 Blade example: Cross-sectional view

### 3. Damages to rotor blades

There are several types of damage that can occur in wind turbine rotor blades. The possible causes of these damages are fabrication inaccuracy, overload and environmental conditions. When regarding the fabrication standards it is obvious which types of failure are encountered. Firstly, bonding failure occurs between all components prefabricated and assembled afterwards. These are lower and upper shell, cylindrical root section (if prefabricated) and webs. Secondly, delamination might occur when resin is not properly injected into the preform. Depending on the location and intensity, delamination might affect the structural integrity as well. In rare cases, when damage growth is not detected early enough, fracture may result.

Damage may also occur due to lightning strike, which is likely to happen at the blade tip. Conducting systems carry electric current up to 1000A from the tip to the ground. When a lightning conductor fails, local temperature spots of more than 1000°C can occur. This results in an explosion of the laminate at the tip area, when humidity expands abruptly. Furthermore, it might also result in a blade fracture. Additionally, erosion is a continuous process affecting the blade's surface layers. Wind, rain, hail, snow and ice are influences that rip off the surface. When the gelcoat loses its homogenous integrity, humidity can penetrate and cause further damage. A similar scenario can develop if longitudinal or transverse cracks occur.

### 4. Theoretical approach for early damage detection

In the 1950s the theoretical approach, which is presented as the basis for early damage detection, was investigated and finally formulated (Rausch 1959). At that time, only a few years after World War II, many buildings that had been severely damaged were repaired in a rough-and-ready way that required knowledge about the integrity of the structures. Special attention was given to the load bearing capability of floors. In 1959 Robert Gasch published the basic approach of the relation between maximum velocity and maximum dynamic stress. Gasch used his suggestion in order to prove that this approach is applicable to concrete floors. The proportionality approach is finally documented within his report on vibration measurements in 1968 (Gasch 1968), which shows the potential of using this approach in order to determine maximum stress amplitudes by measuring the maximum vibration velocity. This proportionality is formulated in Eq. (1). This conception was formulated for uniform beamlike structures with

arbitrary boundary conditions, which are excited near resonance.

$$\sigma_{\text{dyn,max}} = p_{\text{system}} |v_{\text{max}}| \quad (1)$$

For the calculation of the dynamic stress from measured velocity data, the exact knowledge of the proportionality factor “ $p_{\text{system}}$ ” is required. The factor  $p_{\text{system}}$  includes all the information concerning the dynamic behavior of the structure. More specifically, all the parameters in terms of material properties, shape, dimensions, boundary conditions and excitation. The proportionality factor  $p_{\text{system}}$  as introduced by (Gasch 1968, 1966) has the form

$$p_{\text{system}} = \sqrt{E\rho} \cdot p_{\text{profile}} \cdot f_{\text{profile}} \cdot p_{\text{boundary}} \cdot p_{\text{excitation}} \quad (2)$$

The material is represented by the term  $\sqrt{E\rho}$ , which contains the Young’s modulus  $E$  and the density  $\rho$  of the material, whereas the cross section can be specified by Eq. (3), where  $A$  corresponds to the cross section area,  $I$  to the moment of inertia and  $w$  to the section modulus

$$p_{\text{profile}} = \sqrt{\frac{AI}{w^2}} \quad (3)$$

For rectangular cross-sections  $p_{\text{profile}}$  is given by Eq. (4), where  $w$  is the width and  $h$  the height of the cross section

$$p_{\text{rect}} = \sqrt{\frac{wh \frac{wh^3}{12}}{\left(\frac{wh^2}{6}\right)^2}} = \sqrt{3} \quad (4)$$

For thin-walled circular cross-sections  $p_{\text{profile}}$  can be written as

$$p_{\text{circular,thin}} = \sqrt{D^2 - d^2 \frac{4D^2}{(D^4 - d^4)}} \approx \sqrt{2} \quad (5)$$

As the proportionality was derived for rectangular cross-sections, the reference to the basic rectangular shape should be given by the following equation

$$f_{\text{profile}} = \frac{p_{\text{profile}}}{p_{\text{rect}}} \quad (6)$$

The influence of excitation can be described by Eq. (7)

$$p_{\text{excitation}} = \frac{\omega_n}{\Omega} \quad (7)$$

The system is ideally excited in or near resonance. In this case, where  $\Omega \approx \omega_n$ ,  $p_{\text{excitation}} = 1$ . For any other excitation ( $\Omega \neq \omega_n$ ) the factor  $p_{\text{excitation}}$  has to be included, while for the case of free vibration the factor can be assumed to be equal to 1.






For a cantilever beam system, which could be compared to the structure of a wind turbine blade,

the boundary conditions are described by the factor  $p_{\text{boundary}}$  in terms of maximum curvature and maximum amplitude (see Eq. (8)). In Eq. (8)  $\hat{u}_{n,\text{max}}$  is the maximum mode shape curvature and  $\hat{u}_{n,\text{max}}$  is the maximum mode shape deflection.

$$p_{\text{boundary}} = \frac{\hat{u}_{n,\text{max}}''}{\hat{u}_{n,\text{max}}} \quad (8)$$

Due to the fact that the eigenvalue and the curvature of the eigenform are normalized, the factor  $p_{\text{boundary}}$  can be considered to be dimensionless. The factor  $p_{\text{boundary}}$  depends on the static system and the prevailing mode shape, as presented in Table 1.

Table 1 Influence of boundary conditions on  $p_{\text{boundary}}$

Boundary Condition	1 <sup>st</sup> mode	2 <sup>nd</sup> mode	3 <sup>rd</sup> mode
	1	1	1
	1.26	1.33	1.33
	1.325	1.32	1.32
	1	1	1
	0.755	0.75	0.76

The curvature, which is the second derivative of the eigenform of the cantilever beam, can be written as follows, after the introduction of the non-dimensional coordinate  $\xi=x/l$ , where  $l$  is the length of the beam

$$\hat{u}_{n,\text{max}}''(\xi) = -(\lambda_n^2 \cos \lambda_n \xi + \lambda_n^2 \sinh \lambda_n \xi) + \frac{\cos \lambda_n + \cosh \lambda_n}{\sin \lambda_n + \sinh \lambda_n} \cdot (\lambda_n^2 \sin \lambda_n \xi + \lambda_n^2 \sinh \lambda_n \xi) \quad (9)$$

When introducing  $B = \frac{\cos \lambda_n + \cosh \lambda_n}{\sin \lambda_n + \sinh \lambda_n}$  it follows

$$p_{\text{boundary}} = \frac{\hat{u}_{n,\text{max}}''}{\hat{u}_{n,\text{max}}} = \frac{\lambda_n^2 [-(\cos \lambda_n \xi + \sin \lambda_n \xi) + B(\sin \lambda_n + \sinh \lambda_n)]}{\cos \lambda_n \xi - \cosh \lambda_n \xi + B(-\sin \lambda_n + \sinh \lambda_n)} \quad (10)$$

The first eigenform  $\hat{u}_1(\xi)$  and the associated curvature  $\hat{u}_1''(\xi)$  of the cantilever beam are shown in Figs. 3 and 4. Maximum curvature and maximum stress occur at the fixed edge of the beam,

while maximum deflection amplitude and maximum vibration velocity occur at the free end.

To conclude, the main prerequisite for the application of the proportionality method, for the first eigenmode of a cantilever beam, is the synchronized occurrence of maximum deflection and maximum curvature, as shown in Figs. 3 and 4. When considering the structural response under harmonic loading it can be observed that both deflection and velocity are proportional to the dynamic stress. Thus, the mode shape deflection and the dynamic stress must be phase balanced. Velocity, which is used in the proportionality method, is the first derivative of the deflection and is therefore phase shifted to the dynamic stress. Consequently, the major requirement for the original proportionality is fulfilled, when stress and deflection are in phase.

Originally, the proportionality approach was used for avoiding erroneous strain measurements. Here, the proportionality factor is used as a damage indicator. Therefore, vibration velocity as well as stress amplitudes need to be measured directly. Hereby, the change of  $p_{\text{sys}}$  can be considered as an indication for developing damage, since a change of  $p_{\text{sys}}$  means that basic properties of the system have changed. For this purpose  $p_{\text{dam}} = p_{\text{damage}}$  is introduced in Eq. (11).

$$\sigma_{\text{dyn,max}} = p_{\text{dam}} |v_{\text{max}}| \quad (11)$$

The proportionality factor  $p_{\text{system}}$  is measured once at an arbitrary starting time  $t_0$  and describes the initial status of the structure, which is considered to be undamaged. Therewith the initial proportionality factor  $p_{\text{ini}} = p_{\text{system}}$  is introduced. Subsequently,  $p_{\text{system}}$  is recorded continuously. The current proportionality factor is named  $p_{\text{cur}}$ . Its deviation from the initial factor describes the damage as in Eq. (13).

$$p_{\text{dam}} = p_{\text{ini}} - |p_{\text{cur}}| \quad (12)$$

$$\Delta p_{\text{dam}} = \frac{(p_{\text{ini}} - |p_{\text{cur}}|)}{p_{\text{ini}}} \cdot 100\% \quad (13)$$

To ensure that the proportionality factor can be used as an indicator for early damage detection, it is important to verify potential erroneous influences on  $p_{\text{sys}}$ . Recalling Eq. (2) it can be shown that all sub-factors except for  $p_{\text{boundary}}$  are not influenced by damage. In most cases the start of structural damage is a very local incidence. While all sub-factors can be considered to be global parameters of the structure properties,  $p_{\text{boundary}}$  is the only sub-factor that reflects small local effects.

This sub-factor creates a relation between  $\sigma_{\text{dyn,max}}$  and  $v_{\text{max}}$  for a certain eigenform. Regardless of which value changes first, a developing damage in between the points at which these two values are considered, will result in either a change of the stress amplitude due to stress redistribution or in a change of the vibration velocity amplitude. Damage in an early stage neither results in a change of global material parameters such as Young's modulus or density, nor does it result in a change of parameters like moment of inertia or section modulus, which in this case can be characterized as a global parameter as well. This becomes obvious when considering the sub-factor  $p_{\text{profile}}$ . Both  $p_{\text{rect}}$  and  $p_{\text{circular}}$  cannot give information on damage, since only the type of cross section is described. Large damage, which leads to the change of the cross section, is not considered.

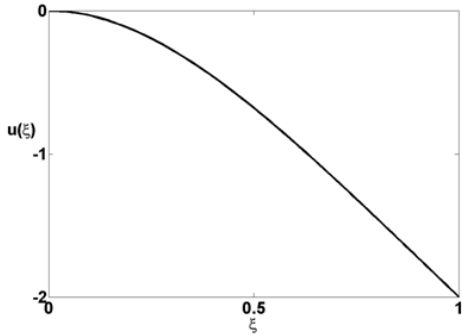


Fig. 3 Eigenform of cantilever beam

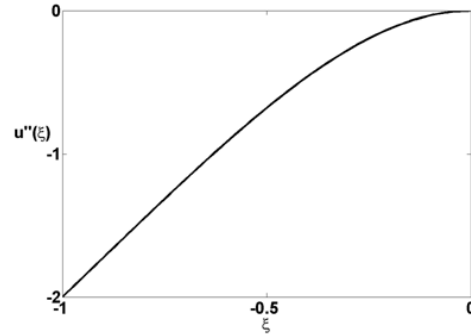


Fig. 4 Curvature of cantilever beam

Furthermore, the influence of  $p_{\text{excitation}}$  can be neglected, since the structures considered, are excited in resonance or will be excited in such a way that they respond in a natural frequency only. Harmonic excitation generates the best results for the proportionality compared to the analytic solution. When using a swept load excitation, which can be compared to the characteristics of strong wind gusts, the results show a slight divergence but are still very close to the results of the analytic solution. As far as the way of applying the proportionality method for damage detection purposes is concerned, it is obvious that it is not necessary that the proportionality factor is determined exactly as described in the theory, because only the relative change of the initial value of  $p_{\text{system}}$  is regarded. This means that the main precondition for the application of the proportionality method does not have to be fulfilled. More specifically, it is not a precondition any more that the structural responses of dynamic stress and deflection occur synchronized. The relative change of two types of sensors at two different positions is observed as the damage indicator, even if these two parameters are out of phase from the beginning.

Temperature could have a bad influence on the parameter  $p_{\text{system}}$ , if not compensated during strain measurement. When related to a reference temperature level, changing temperature conditions affect Young's modulus and the initial total length of the structure. Numerical simulations were performed in order to study whether a changing temperature level has to be considered. A simple uniform cantilever beam was used. Exemplarily, three different temperature levels were investigated. A change in temperature  $\Delta T$  affects the total length of structure by  $\Delta l$  as presented in Eq. (14), where  $\alpha_T$  is the thermal expansion coefficient of the material and  $l_0$  the initial length of the structure (Hoffmann 1987, Thomson 1856)

$$\Delta l = \pm \alpha_T \cdot \Delta T \cdot l_0 \quad (14)$$

This results in a change in both eigenfrequency and the proportionality factor. Table 2 shows the results of the numerical simulations concerning the temperature influence on the proportionality factor  $p_{\text{sys}}$  and eigenfrequency respectively. Consequently, the parameter temperature should be considered, when the proportionality factor is used as a damage indicator. Therefore, it is necessary that the temperature is compensated during field operation of the monitoring system, in order to avoid influences on the proportionality factor.

Table 2 Influence of temperature on 1<sup>st</sup> eigenfrequency and proportionality factor

T[°C]	l <sub>o</sub> [m]	Δf <sub>o</sub> [%]	Δp <sub>sys</sub> [%]
0	0.999	+0.4	+0.12
20	1.000	-	-
100	1.001	-1.38	1.40

## 5. Theoretical derivation of the proportionality method

The derivation of Gasch's proportionality is examined through the analysis of a uniform beam that is subjected to free and forced vibrations. Based on the classical Bernoulli beam theory for vibration problems, the applied load  $F(x,t)$  and the deflection curve  $u(x,t)$  are both functions of space and time. Additionally, the inertia force has to be taken into account. Thus, the equation of motion for the vibrating beam can be written as in Eq. (15), where  $\mu\ddot{u}(x,t)$  is the inertial force,  $EIu''''(x,t)$  represents the elastic restoring force,  $EId_{in}\dot{u}'''(x,t)$  the inner damping (viscoelastic) force and  $d_{out}\dot{u}(x,t)$  the outer damping force, which is proportional to velocity.

$$\mu\ddot{u}(x,t) + EIu''''(x,t) + EId_{in}\dot{u}'''(x,t) + d_{out}\dot{u}(x,t) = f(x,t) \quad (15)$$

Using the Bernoulli product theorem (see Eq. (16))

$$u(x,t) = \hat{u}(x) \cdot T(t) \quad (16)$$

the equation of motion can be split in two differential equations, a space-dependent and a time-dependent. Hence, for a free vibration of a beam the following equation results

$$\mu\hat{u}(x)\ddot{T}(t) + EI\hat{u}''''(x)T(t) + EId_{in}\hat{u}'(x)\dot{T}(t) + d_{out}\hat{u}(x)\dot{T}(t) = 0 \quad (17)$$

The splitting of Eq. (17) results in the two following equations

$$\ddot{T}(t) + \dot{T}(t) \left[ \frac{d_{out}}{\mu} + d_{in}\omega_n^2 \right] + \omega_n^2 T(t) = 0 \quad (18)$$

$$\hat{u}''''(x) - \omega^2 \frac{\mu}{EI} \hat{u}(x) = 0 \quad (19)$$

With the definition of  $k^4 = \omega^2 \frac{\mu}{EI}$  and  $\lambda = k \cdot l$  it follows from Eq. (19) that

$$\lambda^4 = \omega^2 \frac{\mu l^4}{EI} \quad (20)$$

and for the non-dimensional coordinate  $\xi=x/l$ , the general solution of the space-dependent differential equation can be written as follows

$$\hat{u}(\xi) = C_1 \cos \lambda \xi + C_2 \sin \lambda \xi + C_3 \cosh \lambda \xi + C_4 \sinh \lambda \xi \quad (21)$$

Regarding the time-dependent part, the insertion of the complex approach presented in Eq. (22) into Eq. (19) yields the known solution in Eq. (23)

$$T(t) = C e^{\lambda t} \quad (22)$$

$$T_n = e^{-\delta_n t} (A_n \cos \omega_{d,n} t - B_n \sin \omega_{d,n} t) \quad (23)$$

where the decay constant  $\delta_n$  is equal to

$$\delta_n = \frac{1}{2} \left( \frac{d_{out}}{\mu} + d_{in} \omega_n^2 \right) \quad (24)$$

and the eigenangular frequency of the damped system  $\omega_d$  is presented in Eq. (25)

$$\omega_{d,n} = \omega_n \sqrt{1 - \frac{\left( \frac{d_{out}}{\mu} + d_{in} \omega_n^2 \right)^2}{4\omega^2}} \quad (25)$$

Using the Bernoulli product theorem, space and time dependent solutions have to be combined. The result is the space and time dependent free motion equation of the beam due to arbitrary excitation

$$u(\xi, t) = \sum_n \hat{u}_n(\xi) T_n(t) \quad (26)$$

$$u(\xi, t) = \sum_n \hat{u}_n(\xi) e^{-\delta_n t} (A_n \cos \omega_{d,n} t - B_n \sin \omega_{d,n} t) \quad (27)$$

Forced vibration must be considered in order to derive the proportionality of maximum stress and vibration velocity. A modal, complex approach for excitation is employed. Hence, due to the orthogonality of the eigenforms, every force  $F_n$  excites one eigenform  $\hat{u}_n$ . The excitation function in Eq. (28), is thereby developed based on the eigenforms  $\hat{u}_n$ , which comply with the homogenous differential equation (see Eq. (17)) and the boundary conditions required. For an excitation frequency  $\Omega$  the excitation function can be written as follows

$$F(\xi) e^{j\Omega t} = \sum_n F_n \hat{u}_n(\xi) e^{jn\Omega t} \quad (28)$$

The modal, complex approach is

$$u(\xi, t) = \sum_n \hat{u}_n(\xi) T_n(t) \quad (29)$$

with

$$T_n(t) = A_n e^{jn\Omega t}$$

giving the following relations for deflection, velocity and acceleration

$$u(\xi, t) = \sum_n^{\infty} A_n \hat{u}_n(\xi) e^{jn\Omega t} \quad (30)$$

$$\dot{u}(\xi, t) = \sum_n^{\infty} A_n \hat{u}_n(\xi) j\Omega e^{jn\Omega t} \quad (31)$$

$$\ddot{u}(\xi, t) = \sum_n^{\infty} A_n \hat{u}_n(\xi) (-\Omega^2) e^{jn\Omega t} \quad (32)$$

Substituting the excitation term on the right part and the modal, complex approach on the left part of the equation of motion in Eq. (17) and by rearranging the corresponding terms, the complex amplitude factors read

$$A_n = \frac{F_n}{\omega_n^2 \mu \left[ 1 - \frac{\Omega^2}{\omega_n^2} + j\Omega \left( d_{in} + \frac{d_{out}}{\omega_n^2 \mu} \right) \right]} \quad (33)$$

Finally, recalling the amplitudes in Eqs. (30)-(32), the resulting kinematic values of the deflection  $u$ , the vibration velocity  $\dot{u}$  and acceleration  $\ddot{u}$  render

$$u(\xi, t) = \sum_n^{\infty} \frac{\hat{u}_n(\xi) F_n}{\omega_n^2 \mu \left[ 1 - \frac{\Omega^2}{\omega_n^2} + j\Omega \left( d_{in} + \frac{d_{out}}{\omega_n^2 \mu} \right) \right]} \cdot e^{jn\Omega t} \quad (34)$$

$$\dot{u}(\xi, t) = j\Omega \sum_n^{\infty} \frac{\hat{u}_n(\xi) F_n}{\omega_n^2 \mu \left[ 1 - \frac{\Omega^2}{\omega_n^2} + j\Omega \left( d_{in} + \frac{d_{out}}{\omega_n^2 \mu} \right) \right]} \cdot e^{jn\Omega t} \quad (35)$$

$$\ddot{u}(\xi, t) = -\Omega^2 \sum_n^{\infty} \frac{\hat{u}_n(\xi) F_n}{\omega_n^2 \mu \left[ 1 - \frac{\Omega^2}{\omega_n^2} + j\Omega \left( d_{in} + \frac{d_{out}}{\omega_n^2 \mu} \right) \right]} \cdot e^{jn\Omega t} \quad (36)$$

In order to derive the relation between maximum vibration velocity and maximum dynamic stress, it is necessary to introduce the material behavior. Under forced vibration, Hooke's law for an isotropic linear elastic material can be written as

$$\sigma(\xi) = E \cdot \varepsilon(\xi) = -E \cdot u''(\xi) \cdot z \quad (37)$$

and with respect to the viscoelastic damping influence it follows that

$$\sigma(\xi) = E\varepsilon(1 + jd_{fr})\varepsilon = -u''(\xi, t)Ez(1 + jd_{fr}) \quad (38)$$

where

$$d_{freq} = d_{in}\Omega$$

For the computation of the beam's curvature, the deflection of the beam is differentiated twice with respect to variable  $\xi$ . The curvature can then be written as follows

$$\frac{\partial^2 \hat{u}_n}{\partial \xi^2} = \lambda_n^2 \hat{u}_n \quad (39)$$

where  $\lambda_n^2 = \omega_n \sqrt{\frac{\mu}{EI}}$  and  $\mu = \rho A$ .

Introducing the curvature into Hooke's law and for the case of resonance ( $\Omega \approx \omega$ ), where the excited eigenform  $\hat{u}_n$  dominates, Eq. (40) yields

$$\sigma(\xi) = -(1 + jd_{freq})\sqrt{E\rho} \sqrt{\frac{Az_a^2}{I}} \frac{\omega_n F_n \hat{u}_n(\xi)}{\omega_n^2 \mu \left[ 1 - \frac{\Omega^2}{\omega_n^2} + jd_{freq} + j\Omega \frac{d_{out}}{\omega_n^2 \mu} \right]} \cdot e^{j\Omega t} \quad (40)$$

Note that in Eq. (40) the sum of the residual terms of the series expansion has been omitted. Accordingly the velocity is

$$\dot{u}(\xi, t) = j \frac{\Omega}{\omega} \frac{\omega_n F_n \hat{u}_n(\xi)}{\omega_n^2 \mu \left[ 1 - \frac{\Omega^2}{\omega_n^2} + jd_{freq} + j\Omega \frac{d_{out}}{\omega_n^2 \mu} \right]} \cdot e^{j\Omega t} \quad (41)$$

Comparing the maximum stress and the maximum vibration velocity that are presented in Eqs. (42) and (43) respectively, the proportionality condition renders.

$$\sigma_{\max} = \sqrt{E\rho} \sqrt{\frac{Az_a^2}{I}} \frac{\omega_n F_n \hat{u}_{n,\max}}{\omega_n^2 \mu \left[ 1 - \frac{\Omega^2}{\omega_n^2} + jd_{freq} + j\Omega \frac{d_{out}}{\omega_n^2 \mu} \right]} \quad (42)$$

$$\dot{u}_{\max} = \frac{\Omega}{\omega} \frac{\omega_n F_n \hat{u}_{n,\max}}{\omega_n^2 \mu \left[ 1 - \frac{\Omega^2}{\omega_n^2} + jd_{freq} + j\Omega \frac{d_{out}}{\omega_n^2 \mu} \right]} \quad (43)$$

Subsequently, the following expression of the proportionality method derives

$$\sigma_{\max} = \sqrt{E\rho} \sqrt{\frac{A}{I}} z^2 \frac{\hat{u}_{n,\max}}{u_{n,\max}} \left( \frac{\omega_n}{\Omega} \right) \dot{u}_{\max} \quad (44)$$

## 6. Damage detection of blades using the proportionality method

Rotor blades are specifically conceived for the achievement of a high level of effectiveness in terms of costs and aerodynamics, since the rated power output is very much dependent on the aerodynamics of the blades. Before a prototype or optimized design is launched on the market, tests take place, in order to obtain accreditation with regard to the fatigue behavior and critical loads. For this purpose, a fatigue test was performed from January until April of 2009 at the blade test center in Aalborg, Denmark. This test aimed to reach the required accreditation for the blade's optimization, while at the same time the experimental data obtained were used to validate the numerical simulations of the fatigue response of the rotor blade. A 45 m blade was numerically simulated concerning the application of the damage indicator  $p_{\text{dam}}$  on rotor blades of wind energy converters. Similarly to the real test procedure, pure harmonic excitation was applied to the blade. The harmonic excitation was unidirectional and applied to only one location of the rotor blade.

First, a modal analysis was conducted to determine the eigenfrequencies required for excitation. Virtual sensor locations were chosen to calculate the damage indicator  $p_{\text{dam}}$  corresponding to the real sensor locations of the flapwise and edgewise fatigue test. Due to the fact that the area of the blade, which can be accessed by technicians, is restricted by the current blade design, the possible locations for the installation of sensors inside a blade are limited. Therefore, it was investigated whether a sensor must be located at the very tip of the blade when applying the proportionality method for damage detection.

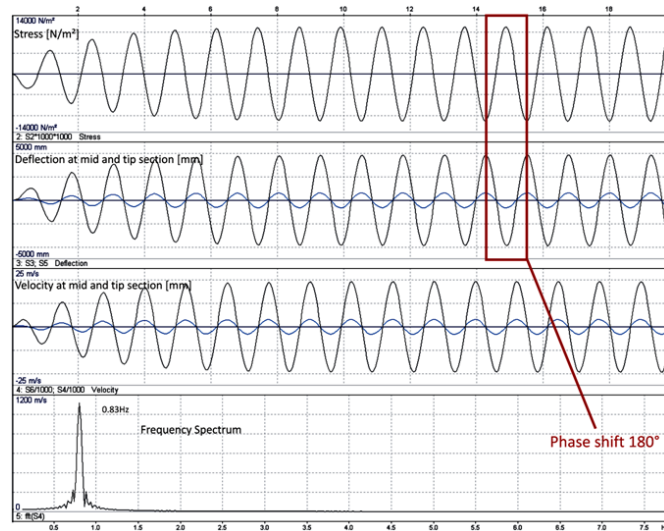


Fig. 5 Plausibility check for the proportionality of the FE-blade model, when using different sensing locations

In Fig. 5(a) comparison of the maximum vibration velocity at the tip and at a mid section location is performed. For comparison purposes, both the deflection at the tip (major amplitude) and the deflection at the mid location (smaller amplitude) were recorded and related to the dynamic stress at the root. It can be observed that proportionality exists and that the signals gained on both locations were “in phase” with respect to the root stress signal.

Despite the fact that the chosen finite element for the stress calculation was located at the lower side of the root section, a negative stress is correlated to a positive deflection and vice versa. This means in this case that the “in phase” characterization is equal to a phase shift of  $180^\circ$ . Since the resulting velocity amplitude for the application of the proportionality method uses the absolute value, the phase shift of  $180^\circ$  can be considered to be equal to  $0^\circ$ . It is worth mentioning that for damage detection purposes through the proportionality method, the phase does not necessarily have to be considered, due to the fact that only a possible relative change of factors  $p_{\text{system}}$  or  $p_{\text{dam}}$  respectively is monitored.

### 6.1 Web debonding scenario

Web debonding is still an important damage feature in rotor blades and usually takes place due to failure of the glue joint. Several reasons cause this damage event such as overload, fatigue or manufacturing. Web debonding may affect structural integrity to such an extent that blade loss may even result. Since the web and the girder are very important components as far as the load carrying mechanism is concerned, it is obvious that high shear stresses are developed between outer shell, girder and web. Web and girders, as well as both shells, are pre-manufactured, and therefore there exists at least one bondline that cannot be finished as carefully as required. This bondline could be characterized as a “blind bondline” because the quality of bonding is doubtful and can hardly be controlled.

In order to examine the performance of the proportionality method for detection of web debonding, several simulations considering different damage lengths were conducted. Initially, these lengths were chosen unrealistically big aiming to check the general performance of the proportionality method at the root, mid and tip sections. Subsequently, these lengths were chosen according to realistic damage cases, which may occur during fatigue tests. Two damage indicators, taken consecutively at 23 m and 40 m, were used for the comparison and estimation of the sensitivity concerning damage detection.

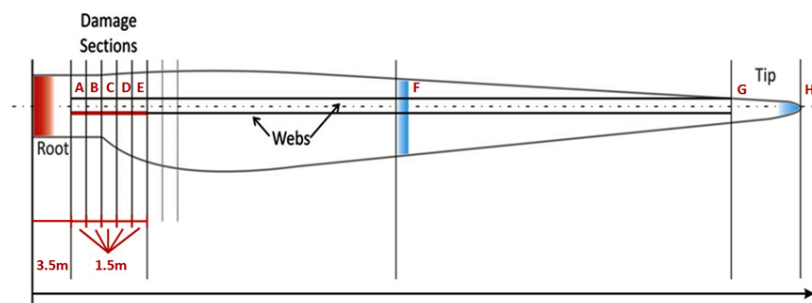
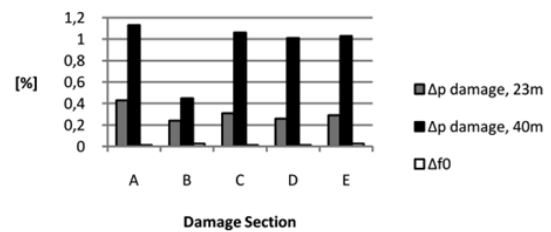


Fig. 6 Overview of damage locations of single sided 1.5 m web debonding (sections A to E) and locations used for the calculation of the damage indicator (sections F and G)

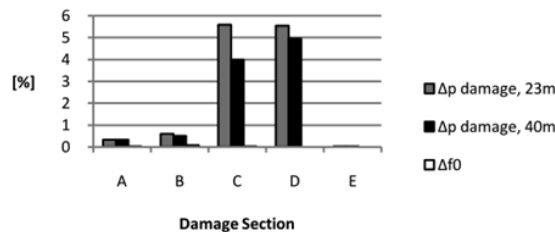
Web debonding was only induced single sided and was limited to a length of 1.5 m at each section. Fig. 6 depicts an overview of the positions of the damage sections. The first damage with a length of 1.5 m was considered at section A, which is located 3.5 m from the beginning of the blade root. Subsequently, 1.5 m damages at each section from B to E were considered. Sections F and G correspond to the two locations used for the calculation of the damage indicators, i.e., 23 m and 40 m respectively. Finally, section H indicates the blade tip, where the maximum velocity occurs.

In Fig. 7(a) the deviation of a 1.5 m single sided web debonding at the root section for excitation in the flapwise direction is presented.  $\Delta p_{\text{dam},23\text{m}}$  roughly varies between 0.2% and 0.4%. On the other hand,  $\Delta p_{\text{dam},40\text{m}}$  is more sensitive, varying between approximately 0.45% and 1.15%. In this case it seems that recording the maximum vibration velocity at the tip section is more effective than recording it at the mid section. Observing the different damage sections chosen, it is conspicuous, as far as the first flapwise mode is concerned, that damage occurring at section B had less influence on the damage indicator than at sections A, C, D and E. The reason is that in this case stress redistribution due to single sided web debonding at section B was not effective enough to significantly change the ratio of maximum stress and maximum vibration velocity. Regarding excitation in the first edgewise mode, a remarkable change in  $p_{\text{dam}}$  only occurred at sections C and D (see Fig. 7(b)). Consequently, an edgewise motion affected these areas much more than the other sections.

The entire structure contributes to the necessary transfer of the bending loads to the root. Especially in the case of edgewise motion the webs are necessary to retain the shape in plane. Thus, shear load is transferred between the shell and the girder and when failure occurs at the connection of these two components stress redistribution is resulted, which is highly dependent on the location of failure. The shell-girder connection in sections C and D are highly loaded during excitation in the edgewise direction, while the blade is vibrating in its first edgewise bending mode. Therefore, the damage indicators in these two locations react significantly.



(a) Flapwise direction



(b) Edgewise direction

Fig. 7  $\Delta p_{\text{dam}}$  due to 1.5 m single sided web debonding at virtual sections A to E

Furthermore, one can observe that in this case the maximum vibration velocity measured at the mid section sensor was a stronger damage indicator than measuring the amplitudes at the tip section. When comparing damage indicator  $p_{\text{dam}}$  to changes in eigenfrequency, it becomes obvious that a change in eigenfrequency due to web debonding was too low, in order to be used for damage indication. A change in eigenfrequency of less than 1% could not be identified reliably, whereas a change in  $p_{\text{dam}}$  over time offered the opportunity to detect changes.

In Fig. 7(b) a significant change in  $p_{\text{dam}}$  at sections C and D is shown. On the other hand the change in eigenfrequency was less than one hundredth of a percent. Compared to sections A, B and E, the sections C and D are highly loaded concerning the first edgewise bending mode, which results in significant stress redistribution. The effect of damage in section E is so small that no significant change could be noticed. Additionally, it can be observed that excitation in the flapwise direction caused smaller changes of the damage factors in comparison to those calculated for excitation in the edgewise direction. Nevertheless, in both cases of excitation the changes in  $p_{\text{dam}}$  were much more significant than the changes in eigenfrequency.

## 6.2 Bondline failure scenario

Similar to web debonding, bondline failure along the bondlines between the upper and lower shell is one of the most often encountered types of damage. The entire bending and torsional motion of the blade is transferred from the aerodynamic shape sections to the cylindrical root section. Additionally, bondlines are affected significantly by ovalization loads. Under these conditions bondline failure may soon develop and reach a serious size and even result in a total loss of the blade, in case the damage is detected too late. Therefore, it has to be detected as soon as possible, in order to prevent dangerous situations. Figs. 8 and 9 show schematically the bondlines along the leading and trailing edge respectively.

Especially the transition section from cylindrical to aerodynamic shape is very likely to fail. The transition plate serves for the reduction of the blade width from the aerodynamically shaped sections towards the root section within a few meters. In contrast to the aerodynamically shaped sections of the blade, the cylindrical root section shows a high laminate thickness, in order to carry the loads to the hub. Hence, due to the thickness the bondlines within the cylindrical sections are very unlikely to fail.

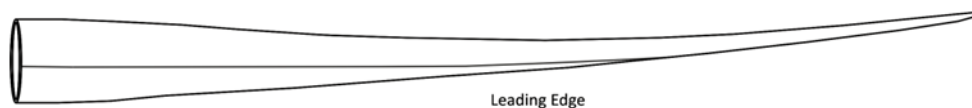


Fig. 8 Side view of bondline along leading edge

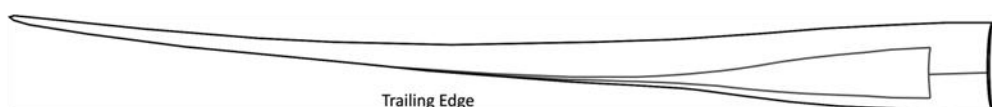


Fig. 9 Side view of bondline along trailing edge

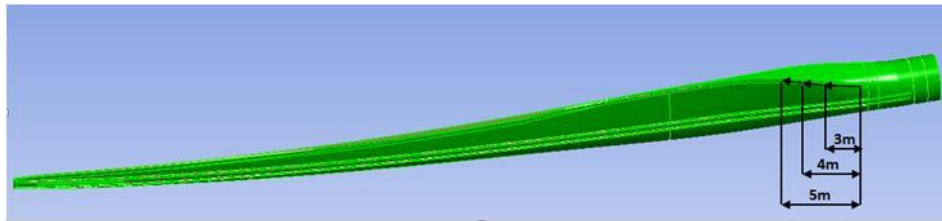
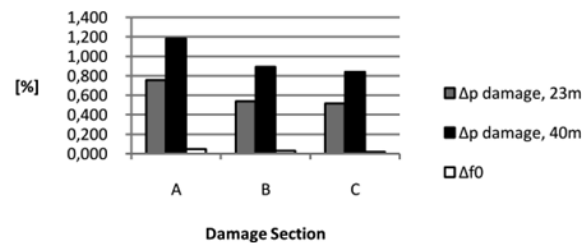
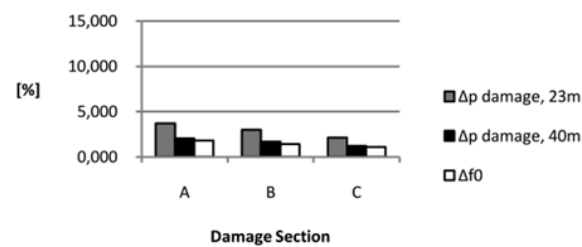


Fig. 10 Overview of damage sections along the lower trailing edge



(a) Flapwise direction



(b) Edgewise direction

Fig. 11  $\Delta p_{\text{dam}}$  due to lower trailing edge bondline failure at sections A, B and C

Numerical simulations were performed in order to investigate the effects of bondline failures on eigenfrequency and on the damage indicator  $p_{\text{dam}}$ , starting with a bondline failure of 1 m. Regarding the results of the numerical simulations concerning bondline failure, it has to be mentioned that the use of the proportionality method offered a much better possibility of detecting this type of blade damage than only observing the change in eigenfrequency. Independent of the locations of the induced virtual damage, all case studies could show that the damage indicator  $p_{\text{dam}}$  was more sensitive than the eigenfrequencies.

For the determination of the optimal locations for the placement of the novel deflection sensor investigations were required. Depending on the direction of vibration, more significant results could be observed from the use of  $p_{\text{dam}}$  at 23 m or  $p_{\text{dam}}$  at 40 m. Figs. 10-15 show the maximum indication of bondline failures depending on the damage location and the damage length. When the blade is excited in the flapwise direction it does not react significantly to bondline failure with regard to eigenfrequency. This applies to debonding of both leading and trailing edge.

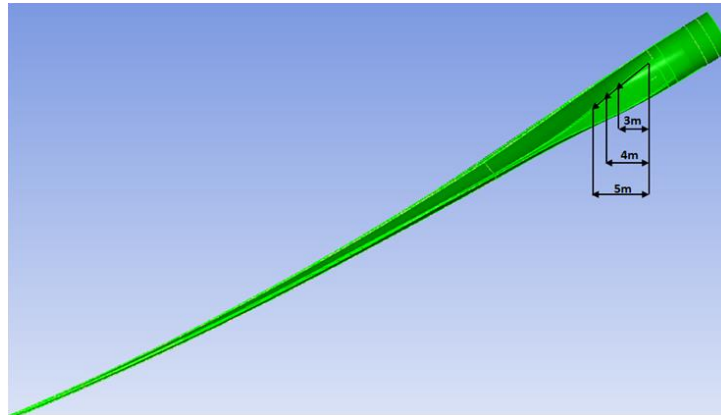


Fig. 12 Overview of damage sections along upper trailing edge

For the lower trailing edge area three sections needed to be investigated. More specifically, maximum damage lengths of 3 m (section C), 4 m (section B), and 5 m (section A) were induced, as depicted in Fig. 10. It can be noticed that damage in section A resulted in the most significant changes in damage indicator  $p_{\text{dam}}$ , regardless of the flapwise or edgewise motion (see Figs. 11(a) and 10(b)). Furthermore, all the analyses showed that the eigenfrequency decreases significantly less than the damage factors.

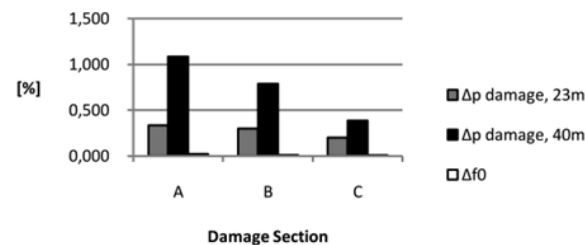
For the upper trailing edge damage scenario maximum damage lengths of 3 m (section C), 4 m (section B) and 5 m (section A) were introduced at slightly different positions from the root (see Fig. 12). The results of damage indication using the proportionality method for the flapwise motion presented significant changes when compared to the eigenfrequency (see Fig. 13(a)). For the case of a 5 m damage,  $p_{\text{dam},40\text{m}}$  changed by 1.181% of the initial value, while the eigenfrequency decreased only by 0.047%. The results of damage indication for motion in the edgewise direction, which are shown in Fig. 13(b), indicated more significant changes in comparison to the reference state. In this case the virtual sensor located at 23 m showed the maximum deviation. For this specific scenario the eigenfrequency decreased approximately the same as the damage indicator  $p_{\text{dam},40\text{m}}$ .

The last case of bondline failure examined was along the leading edge of the rotor blade. The maximum damage lengths introduced were chosen to be 3 m (section C), 4.5 m (section B) and 6 m (section A), as presented in Fig. 14. The leading edge transition from cylindrical to aerodynamic shape is smoother than that at the trailing edge. For damage along the leading edge, the damage indicator  $p_{\text{dam}}$  was again more sensitive to damage than the eigenfrequency (see Figs. 15(a) and 15(b)). Furthermore, as seen before for debonding at the trailing edge, motion in edgewise direction showed much higher sensitivity.

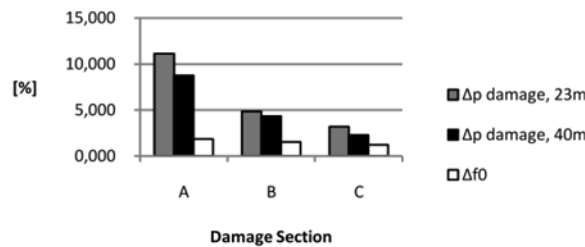
It can be concluded that when the blade was affected by any type of bondline failure, the edgewise direction offered the best performance for damage detection. In all cases investigated, the parameters used for detection showed quite significant results, regardless of leading or trailing edge. It can be seen that very significant changes were resulted, when the bondline failed within the observed special ranges. The reason can be found in the trailing edge construction, which results in intense stress redistribution, when the loads, due to damage, cannot be properly

transferred to the root. For the flapwise motion the magnitude of the damage indicator  $p_{\text{dam}}$  was much larger than the change of eigenfrequency. However, the magnitude of the damage indicator  $p_{\text{dam}}$  was lower as compared to edgewise motion.

As mentioned earlier the numerical analyses were conducted at the same time with a fatigue edgewise test in Aalborg, during which a damage of 1.5 m length was induced on the upper shell trailing edge bondline. The length of this induced damage increased and reached 2 m length, until the test was stopped for safety reasons. Therefore, the results of a more specific numerical analysis that present the spreading of a corresponding bondline failure are presented, in order to be able to compare the behavior of the damage factor occurring from this analysis to the behavior of the damage factor calculated during the test.



(a) Flapwise direction



(b) Edgewise direction

Fig. 13  $\Delta p_{\text{dam}}$  due to upper trailing edge bondline failure at sections A, B and C

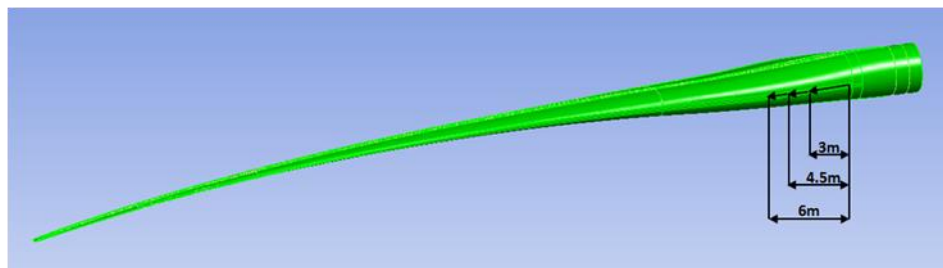
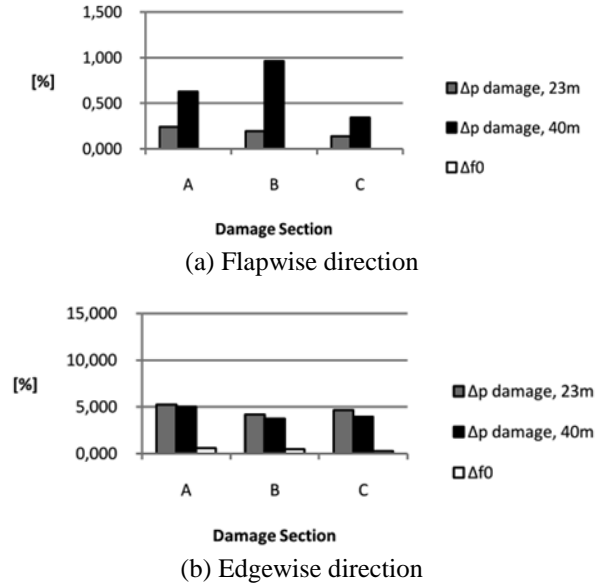


Fig. 14 Overview of damage sections along the leading edge

Fig. 15  $\Delta p_{\text{dam}}$  due to leading edge bondline failure at sections A, B and CTable 3  $\Delta p_{\text{dam}}$  at 23 m and 40 m and change of eigenfrequency due to an increasing upper trailing edge bondline failure

Edgewise Direction	$f_o$ [Hz]	$\Delta f_o$ [%]	$\Delta p_{\text{dam},23\text{m}}$ [%]	$\Delta p_{\text{dam},40\text{m}}$ [%]
Reference State	1.4111	-	-	-
0.5 m Damage	1.4094	0.122	0.454	0.153
1.0 m Damage	1.4040	0.503	0.993	0.414
2.0 m Damage	1.3990	0.857	1.774	0.942
3.0 m Damage	1.3931	1.276	2.355	1.414
4.0 m Damage	1.3893	1.545	3.329	1.828
5.0 m Damage	1.3858	1.793	3.717	2.038

Starting at a location 5.1 m from the root of the blade, a 0.5 m bondline failure along the upper bondline of the trailing edge was introduced. After reaching 1 m, this failure was grown meter by meter up to a total length of 5 m. Table 3 shows the results for the damage indicator  $p_{\text{dam}}$  at 23 m and 40 m respectively and for the eigenfrequency under excitation in edgewise direction. The damage indicator  $\Delta p_{\text{dam},40\text{m}}$  changed slightly more than damage indicator  $\Delta p_{\text{dam},23\text{m}}$ , while the eigenfrequency was again not influenced significantly. It can be observed that a damage of 2 m caused a reduction of  $\Delta p_{\text{dam},23\text{m}}$  of 1.774%.

## 7. Test-site measurement of a 50.8 m blade

### 7.1 Description of test and sensor concept

Each newly developed or modified blade must be certified in terms of dynamic durability and strength under high static loads. Currently there are only three facilities in Europe capable of performing static tests and dynamic fatigue tests in order to document the quality of the blade. Static and dynamic tests are performed in the flapwise and edgewise direction of the blade. Certain amplitudes and bending moments at certain positions have to be achieved for a defined duration or number of cycles. When necessary, additional load is applied by steel elements, which are clamped on the outer shell of the blade (Germanischer Lloyd Rules and Guidelines VI 2007).

A 50.8 m blade was tested in a test facility in Aalborg, Denmark, where an edgewise fatigue test ran for more than 4 million cycles. This test started in January and ended in April 2009. The whole test procedure was observed and the consistency of the proportionality factor  $p_{\text{dam}}$  was shown and can be seen in the results. An unbalanced exciter was used to apply a dynamic load to the blade. In this case, an amplitude of approximately  $\pm 100$  mm in the edgewise direction could be measured at 23 m from the root.

The blade was equipped with a four-sensor-chain of fiber optical strain gauges (FOS) placed in the root area of the blade and oriented in the longitudinal direction. Additionally, the blade was equipped with two novel sensor prototypes measuring deflections at parallel positions, on the inside of the blade and at a distance of 23 m from the root section (see Fig. 16). Two deflection sensors were used for redundancy and accuracy purposes. For each combination of optical strain gauge and deflection sensor a separate proportionality factor was calculated. Deflection was used as the initial value for determining the vibration velocity, since calculating the vibration velocity by the first derivative of the deflection signal, is more accurate than the integration of acceleration data. HBM together with Vanderhoek-Photonics developed this new type of sensor, which was optimized for wind turbine blade applications. This sensor can be mounted along the webs inside the blade and is completely insensitive to lightning strikes, as no metallic or wiring components are included inside the blade. The basic assembly is presented in Fig. 17.

Both sensor units have to be stably connected to the web, as a mean rotational speed of approximately 10 to 12 revolutions per minute causes high centrifugal forces. Therefore, special fiber patches were manufactured, which are laminated to the webs and are used as sensor feet. The basic sensing system is inserted to the active unit. Directly behind the location of string fixation to the web, two load cells are carefully connected to the string. Both cells are orientated orthogonally. A change of string angle is recorded as voltage per millimeter (V/mm).

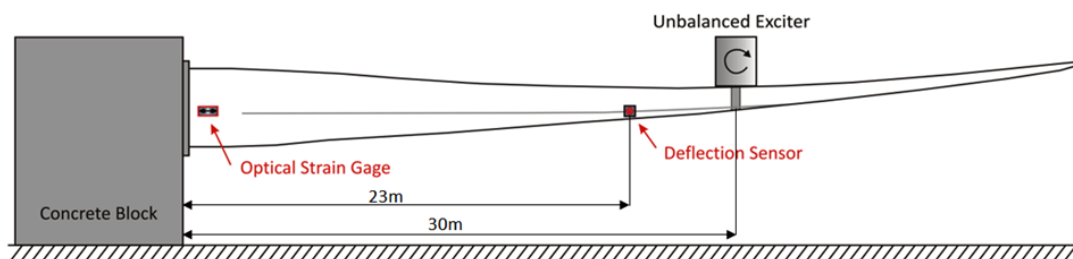


Fig. 16 Schematic diagram of sensor locations for edgewise test

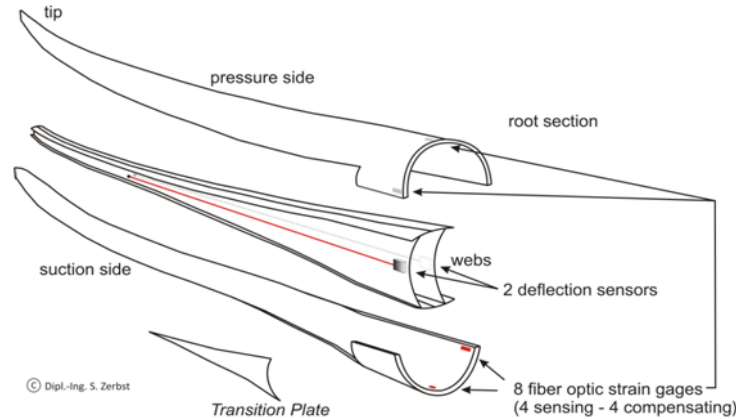


Fig. 17 Schematic sketch of the principle of the new deflection sensor

## 7.2 Application of the proportionality method within a fatigue test

An edgewise fatigue test was performed on a 50.8 m rotor blade by applying 4 million cycles in the edgewise direction. The blade was thus equipped with many additional masses at several locations along its longitudinal axis, in order to reach the required strain values. The structure was excited in resonance using an unbalanced exciter, which was fixed on the blade's top side (suction side). The test started on the 22<sup>nd</sup> of January and the initial excitation frequency was adjusted to be  $\Omega=1.123$  Hz. This value complies with the first eigenfrequency (bending mode) in edgewise direction.

Due to the precurvature and the limited space inside of blade the deflection sensor could not be installed further than 25 m from the root. Therefore, no measurement data of the vibration velocity at the tip were recorded. Considering only the damage indicator  $p_{\text{dam}}$  it is sufficient to rely on a factor recorded 23 m from the root, where both deflection sensors were fixed on the web. As a result of the varying cross-section over the length and the resulting differences in stiffness, the overall deflection was characterized by a multiaxial motion. Therefore, despite the fact that the excitation takes place in the edgewise direction, the blade moves in the flapwise direction as well. The global motion can be described as a tumbling motion with the blade tip following an elliptical orbit.

The fact that the blade's cross section is everywhere non-symmetric, except for the cylindrical cross section at the root, resulted in two different proportionality factors  $p_{\text{sys}}$  in each the edgewise and flapwise directions. The deflection sensor at the trailing edge was combined with the trailing edge strain gauge and the deflection sensor at the leading edge was combined with the leading edge strain gauge. As an alternative, this could also be cross-correlated, using for instance the leading edge deflection sensor in combination with the trailing edge strain gauge and vice versa. During edgewise excitation the leading and trailing edge are loaded differently, resulting in different levels of stress and strain. However, the deflection amplitude at 23 m showed only small differences, when comparing the leading and trailing edge signals.

From the measured values of vibration velocity at 23 m recorded at the initial testing time, a current edgewise proportionality factor could be identified. The average edgewise proportionality

factor was determined to be

$$p_{sys, meas} = 104.424 \frac{MNs}{m^3}$$

Due to the non-uniform cross-section of a turbine blade, the stiffness in the two moving directions differed. Obviously, four different proportionality factors resulted: two for the edgewise and two for the flapwise direction, because each optical strain gauge was combined with the related deflection sensor axis. Consequently, the leading edge strain gauge was combined with the measurement of the deflection sensor in the horizontal axis, in order to create the leading edge proportionality factor. The same holds for the calculation of the trailing edge proportionality factor. With respect to flapwise motion, redundancy is offered by two combinations for the suction and two for the pressure side respectively. Nevertheless, only the consideration of one of these two combinations is sufficient.

As far as the estimated and the measured value of  $p_{sys}$  are concerned, it must be mentioned that these two values should not necessarily coincide. It is important that the sensor positions remain constant during the tests and as long as this requirement is fulfilled, the relative monitored change in  $p_{sys}$  or  $p_{dam}$  can be used to detect damage reliably.

After the regular fatigue test was successfully completed, a trailing edge bondline failure was introduced manually by cut-off. A damage length of 1.5 m at the upper trailing edge of the transition section was applied and the fatigue test was restarted. This section, where the aerodynamic cross section changes to a cylindrical cross section, is characterized by two main bondlines (upper and lower) which are highly loaded due to the edgewise motion. Within 24 hours of testing after damage induction, a significant increase in damage could be noticed elongating the upper trailing edge failure. This damage growth could be detected with respect to the reference state recorded during the first edgewise test. The initial damage of 1.5 m length reached approximately 2 m length in a short period of time. Therefore, due to safety reasons the fatigue test had to be stopped.

### 7.3 Results

In Fig. 18 the time history of the damage indicator  $p_{dam}$  over 4.3 million cycles performed during edgewise testing is presented. The history of the proportionality factor from the beginning of the test until state 1 presents the development of the damage indicator from the initial undamaged state until the damaged state and the shutdown of the experiment. Red line 1 indicates that the test had to be shut down due to the existence of an intense damage. According to the information by the manufacturer, the occurring deviation of 2.45% from the initial value of the factor seemed to be reasonable, when compared to the results of the numerical simulations. In section 6.2 the results of the numerical analysis for the case of upper trailing edge bondline failure were presented. For the damage factor  $\Delta p_{dam, 23m}$  a decrease of 1.774% was calculated when moving from 1 m damage to a damage of 2 m length. This decrease approximates the decrease of the damage factor that was calculated during the test.

After the test had been shut down, the damaged areas were repaired. Both damage indicators  $p_{dam}$  changed suddenly, having completely different levels compared to the reference state. The level increased by 31% and 35%, which can be explained by the structural change due to repair work, since neither sensor configurations, nor extra mass distribution on the blade had changed.

The dashed line in Fig. 18 presents the difference between the state of  $p_{\text{dam}}$  factor at the moment when the test was stopped and the state after reparation. Before the fatigue test was stopped both damage indicators  $p_{\text{dam}}$  underwent a sudden decrease after having temporarily increased. It is likely that the deformation of the cross section became very high. This assumption is underlined by the visual inspections inside the blade, while the fatigue test was in progress.

After repair the test was restarted and was completed without any unscheduled incidents. It can be observed that both damage indicators were subjected to changes until 4.3 million cycles had been reached. This could indicate further damage but such an event was not verified in detail by the manufacturer. It was stated that a web debonding located at the beginning of the web at the root section took place, but did not reach significant dimensions. The fact that no further repair was necessary, gives unfortunately no information about damage intensity. Despite the fact that the values of both damage indicators changed until the completion of 4.3 million cycles, there was no abrupt decrease of the factors values, such as in line 1, where damage occurred. Comparing to the numerical results of the damage scenario of web debonding, it seems unlikely that within the edgewise motion, damage could occur significantly at this specific position, because this type of damage generally caused greater changes of the edgewise proportionality factor, when it occurred further away from the root.

In the period after restart and more specifically between states 2 and 3 of Fig. 18, both levels of  $p_{\text{dam}}$  for the trailing and leading edge changed by 6.86% and 4.52% until the completion of 4.3 million cycles. Another reason for the deviation of the damage factors could be the fact that the eigenfrequency changes during the test. In Table 4 the percentile deviation of the damage factors  $p_{\text{dam}}$  for the trailing and leading edge from the initial state and from the restart state, as well as the percentile change of the excitation frequency  $\Delta\Omega$  are presented. In Table 4 the deviations that refer to the initial state are indicated with (1), while the deviations that refer to the restart state are indicated with (2). These changes should be compared to the total change during the test of the first bending mode in the edgewise direction. The initial excitation frequency was compared to the excitation frequency at the end of the tests and a divergence of 2.1% was found. Consequently the excitation frequency, which automatically self-adjusted over the testing time, changed from  $\Omega_{\text{start}}=1.123\text{Hz}$  to  $\Omega_{\text{end}}=1.099\text{ Hz}$ . Despite the existence of some peaks in the time history of the damage indicators that could be interpreted as damage, these could unfortunately not be related to any structural changes. Nevertheless, no abrupt decrease of the damage factors as in line 1 could be observed.

This measurement campaign, as well as the numerical studies concerning the detection of different damage scenarios showed that it is not essentially necessary to use the maximum vibration velocity amplitude as an input parameter for the application of the proportionality method. It was shown that depending on the damage location, even a position for sensing vibration velocity closer to the root of the system may react more sensitive than the original position based on Gasch. Additionally, it must be emphasized that  $p_{\text{dam}}$  can only be considered as a global damage indicator. This factor is neither able to give information about the damage location nor able to give information about the exact damage intensity.

Concluding, during the edgewise fatigue test a damage of 1.5 m length was successfully detected by the decrease of the damage factor and the further spreading of the damage was also visible in the behavior of the damage factor. In addition, the percentage decrease of the damage factor due to the spreading of the damage at the upper trailing edge bondline from 1.5 m to 2 m (2.45%) is comparable to the decrease of the damage factor that occurred from the numerical analysis of the same damage scenario for the spreading of damage from 1 m to 2 m (1.774%).

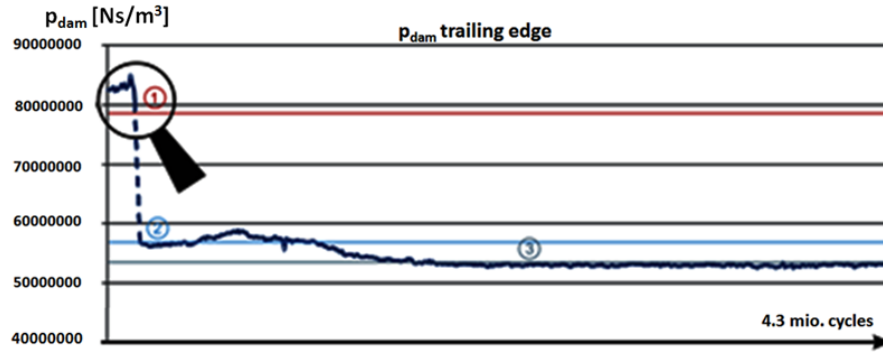


Fig. 18 Time history of  $p_{\text{dam}}$ , recorded from the trailing edge deflection sensor (edgewise testing). States 1, 2 and 3 indicate test stop due to damage, test restart and arbitrary moment after blade repair respectively.

Table 4 Percentile deviation of damage factors  $p_{\text{dam}}$  during the edgewise fatigue test

Incident	Trailing Edge Deviation [%]	Leading Edge Deviation [%]	$\Delta\Omega$ [%]
1	2.45 <sup>(1)</sup>	1.71 <sup>(1)</sup>	0.0
2	31.07 <sup>(1)</sup>	35.52 <sup>(1)</sup>	2.1 <sup>(1)</sup>
3	6.86 <sup>(2)</sup>	4.52 <sup>(2)</sup>	2.1 <sup>(1)</sup>

## 8. Conclusions

A novel approach for early damage detection in wind turbine blades was presented, which is based on a theory originally applied to stress determination on floor slabs by only measuring the vibration velocities. This approach was at that time developed for uniform beamlike structures, but was able to be extended to non-uniform beamlike structures. It can be concluded that the proportionality method shows higher sensitivity to damage than the observation of the changes of the eigenfrequencies.

A numerical model of a 45 m blade was used in order to investigate the efficiency of this approach for early damage detection for different types of damage scenarios. Therefore, damages that are likely to occur due to manufacturing inaccuracy were chosen. At the same time, a real 50.8 m turbine blade was used for investigations during an edgewise fatigue test on a test-site in Aalborg, Denmark. During these tests a sensor prototype was used for the measurement of the deflection. This prototype is characterized by the advantage that no metallic components or wiring have to be installed inside the blade, offering high security against lightning. This fact in combination with the indications of a very good performance in terms of sensitivity and reliability, make the deflection sensor applicable to blade monitoring. Additionally, a further advantage of the use of this deflection sensor in early damage detection is the fact that the determination of

vibration velocity is conducted by signal differentiation, a process which is more accurate than the integration of acceleration data, which can be measured from accelerometers. In combination with the installed optic strain gauges, the entire system could show its high quality and adequacy within this application in wind turbine rotor blades. Before the start of a second edgewise test, a cut along the trailing edge was introduced, which was successfully detected by the application of the proportionality method. The increase of the damage during the edgewise test could also be detected by the proportionality factor data over time. The results of the test measurements coincided with the results of the numerical analyses. It was concluded that the proportionality method is appropriate for early damage detection for different possible damage scenarios. Compared to the change of eigenfrequency due to damage, the proportionality method offers a more sensitive performance relying on two different kinds of sensor types. Nevertheless the robustness with respect to noise has to be evaluated.

Further research is required for the case of excitation of the rotor blade at frequencies other than the first eigenfrequency, i.e., for colored noise input excitation. The signals may be filtered close to the eigenfrequencies, so that the influences of other frequencies are minimized, and consequently the proportionality method may be applied. The signal-to-noise ratio has to be taken into account for the case of non-harmonic excitation, such as the excitation of the blades during the operation of a wind turbine.

## References

- Ashley, F., Cipriano, R.J., Breckenridge, S., Briggs, G.A., Hinkson, J. and Lewis, P.A. (2007), *Bethany wind turbine study report*, [www.townofbethany.com](http://www.townofbethany.com).
- Caithness Windfarm Information Forum (2010), Summary of wind turbine accident data to 30th September 2010, [www.caithnesswindfarms.co.uk](http://www.caithnesswindfarms.co.uk), accessed 2010.
- Claus, F. (2007), *Abgebrochener Rotorflügel segelt über Landstraße*, Lausitzer Rundschau, Mai, [www.lr-online.de](http://www.lr-online.de).
- Gasch, R. (1966), *Sammlung und Auswertung von Erschütterungsmessungen*, Berlin.
- Gasch, R. (1968), *Eignung der Schwingungsmessung zur Ermittlung der dynamischen Beanspruchung in Bauteilen*, Ph.D. Dissertation, Technische Universität Berlin, Berlin.
- Gasch, R. and Tvele, J. (2007), *Windkraftanlagen*, (5th Ed.), Teubner, Wiesbaden, Hesse, Germany.
- Germanischer Lloyd (2007), *Guideline for the Certification of Condition Monitoring Systems Edition 2007*, Rules and Guidelines IV, Industrial Services, Hamburg.
- Hahn, B., Durstewitz, M. And Rohrig, K. (2006), *Reliability of Wind Turbines*, ISET, Kassel, Germany.
- Hoffmann, K. (1987), *Eine Einführung in die Technik des Messens mit Dehnungsmessstreifen*, Hottinger Baldwin Messtechnik GmbH, Darmstadt, Hesse, Germany.
- Rausch, E. (1959), *Maschinenfundamente und andere dynamisch beanspruchte Baukonstruktionen*, VDI-Verlag, Düsseldorf, North Rhine-Westphalia, Germany.
- Thomsen, O.T. (2009), "Sandwich Materials for Wind Turbine Blade – Present and Future", *J. Sandwich Struct. Mater.*, **11**(1), 7-26.
- Thomson, W. (1856), *On the electro-dynamic Qualities of Metals*, Philosophical Transactions of the Royal Society of London, London.
- Wind Watch (2010), [www.wind-watch.org/documents/wp-content/uploads/fullaccidents.pdf](http://www.wind-watch.org/documents/wp-content/uploads/fullaccidents.pdf), accessed 2010